The investigation of direct current microdischarges in HgCdTe -coupled Ar/H_2 gas medium at atmospheric and hyper-atmospheric pressures

HATICE HILAL YÜCEL (KURT)*, SELÇUK UTAŞ, ERHAN ONGUN
Department of Physics, Faculty of Science, Gazi University, Ankara, Türkiye

The rapid development of semiconductor materials in recent years has enabled the use of semiconductors as photodetectors in the field of infrared (IR) sensing and imaging applications. In the near-IR region, HgCdTe (MCT) is useful in remote sensing systems with its high quantum efficiency, high sensitivity, high photon detection capacity, minimal photon loss and long wavelength heterojunction photodiode features. MCT semiconductor material continues to be intensively developed and used in various fields of optoelectronics since its synthesis in 1958. This conceptual research study aimed to identify the unique transition regimes between electron emission and electrical breakdown states in gas discharge-semiconductor microplasma systems (GDSS), and to truly establish the basis for modeling highly efficient infrared-visible image converter devices for advanced optoelectronic applications. A MCT material -coupled direct current glow-discharges were numerically studied and reported with unique surface plasma patterns across 100 μm gap in binary argon/hydrogen (Ar/H_2) gas model, where H_2 is added to Ar at 10% molar fraction. Theoretical analyzes were also carried out to investigate and compare the effects of atmospheric and hyper-atmospheric pressures of binary Ar/H_2 gas models on the spatiotemporal key discharge parameters. Numerical analysis results of the spatiotemporal discharge parameters including, electron density (ED), electron energy density (EED), and electron current density (ECD), obtained from the proposed GDSS simulation models, have revealed that a significant contribution can be made to increasing ion-induced secondary electron emission (SEE) yield in hydrogen-added argon gas medium at hyper-atmospheric pressure.

(Received November 1, 2023; accepted June 5, 2024)

Keywords: Glow discharge, Microplasma, Infrared, Photodetectors, $Hg_{1-x}Cd_xTe$, Ar/H_2, Simulation

1. Introduction

Recent studies have been reported on the theoretical and experimental investigation of planar DC field-driven gas discharge-semiconductor systems (GDSS) [1-8] for modeling highly efficient infrared (IR)–visible (VIS) image conversion applications.

In this paper, an exclusive focus has been placed on the HgCdTe or MCT semiconductor material [9-11]. MCT is one of the preferred choices for all current infrared (IR) focal plane array (FPA) technology [12, 13]. Contrary to the universally followed path for the last 20 years, the optimum diode architecture is N+/P. It is not P+/N, which allows the lowest dark currents and hence the highest operating temperatures of all known IR material technologies and avalanche recovery capability [14]. It can be said that HgCdTe has made significant advances in FPA technology and is currently the dominant material technology in all IR spectral bands. $Hg_{1-x}Cd_xTe$ (x=0.2) is a heterojunction compound semiconductor operating in the near infrared region [15].

HgCdTe (MCT), a tunable infrared photodetector material, is a chemical compound in zincblende structure with a cubic lattice formed by combining them in certain proportions [16, 17]. Fig. 1 shows the crystallographic zincblende structure of (a) HgCdTe unit cell with (b) tetrahedral environment of Hg atom surrounded by Te atoms.

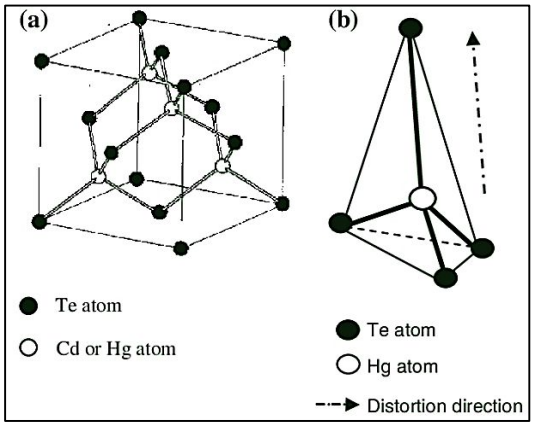

Fig. 1. (a) Crystallographic zincblende structure of HgCdTe unit cell, (b) tetrahedral environment of Hg atom surrounded by Te atoms [16]

Fig. 1 shows the crystallographic structure of a unit cell of HgCdTe heterojunction compound semiconductor material [16]. For operation in different infrared ranges, Cd ratio in the compound is changed. CdTe is a semiconductor with a band gap of about 1.5 eV [18], and HgTe is a semimetal with a zero-band gap. The adjustable

bandgap of HgCdTe, formed by the combination of these two compounds, is set between 0-1.5 eV which corresponds energies of infrared light spectrum [19].

In HgCdTe the mean free path of electrons can be several micrometers long. HgCdTe is a soft material due to the Te and Hg elements in its composition. HgCdTe has low thermal conductivity which means it is not suitable for high power devices [20]. The infrared operating wavelength range lies between 3 to 5 μm (medium wave infrared window, MWIR) and 8 to 12 μm (long wave window, LWIR) [21].

Fig. 2 introduces infrared photodetector materials in the wavelength scale from 760 nm to 300,000 nm, which lies between the edges of near-infrared (NIR) and far-infrared (FIR) bands, where the spectral placement of HgCdTe material is shown.

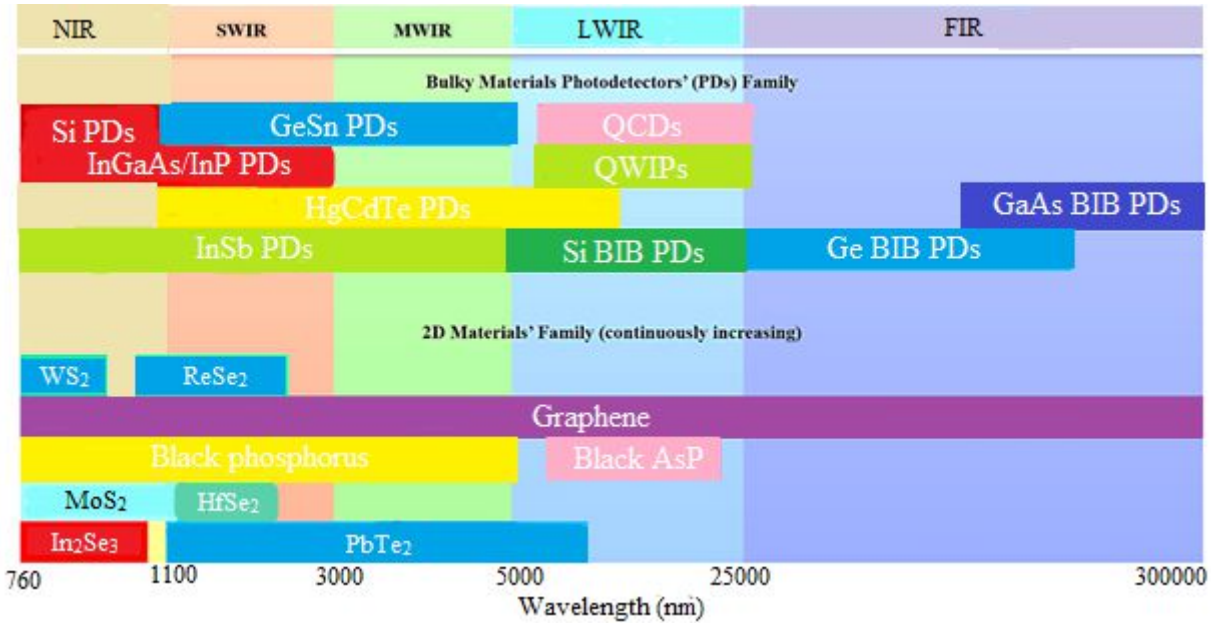

Fig. 2. The spectral placement of HgCdTe semiconductor material across the long range of NIR, SWIR, MWIR, and LWIR spectra [22] (color online)

Electrical breakdown occurs due to the combination of electron emission and ionization. The well-known Townsend breakdown criterion established the relation between the secondary electron emission (SEE) coefficient γ_{SE} and electron avalanche ionization, governed by the number of ionizations per unit length α, where d is gap distance:

$$\exp(\alpha.d) - 1 = \gamma_{SE}^{-1} \quad (1)$$

Eq. 1 describes that secondary electron emission plays in driving breakdown by this Townsend avalanche (TA). For a given discharge gap with a specified background gas and gap geometry, spatially and temporally resolved numerical simulations can predict the discharge process and determine the breakdown condition [23]. Fig. 3 shows that field emission-produced ions subsequently interact with the cathode to release more electrons (SEE).

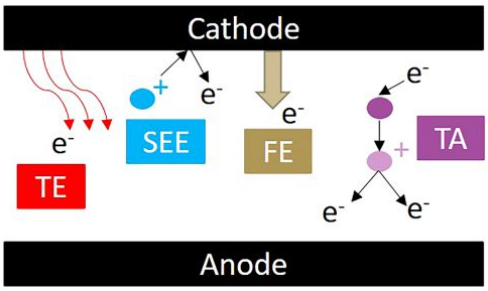

Fig. 3. Schematic of the mechanisms involved in microscale gas breakdown including, thermionic emission (TE), ion-induced secondary electron emission (SEE), field emission (FE), and collisions (TA) [23] (color online)

Introducing an additional contribution of γ' to γ_{SE} that modifies Eq. 1 to Eq. 2:

$$\exp(\alpha.d) - 1 = (\gamma_{SE} + \gamma')^{-1} \quad (2)$$

Several research articles have recently outlined solutions to these equations for gas breakdown mechanisms using numerical methods [24-26]. Numerical methods are important tools for improving our knowledge of plasma behavior in micro discharge cells coupled with semiconductor cathode materials, and are also crucial for increasing our knowledge in the field of deposition or etching [27-29].

The characteristic current/voltage curve of typical gas discharges, which reveals the dark discharge, glow discharge and arc discharge regimes [30, 31], is used to define the approximate operating point of a GDSS.

The breakdown characteristics of DC hydrogen discharges were investigated for micro gaps [32].

With this motivation, this conceptual research study aimed to identify the unique transition regimes between electron emission and gas breakdown mechanism across 100 μm gap, and to truly model the basis for highly efficient infrared-visible image converter devices for advanced optoelectronic applications. Theoretical analyzes were carried out to investigate and compare the effects of atmospheric and hyper-atmospheric pressures of hydrogen-added argon binary gas system on the spatiotemporal variations of key discharge parameters including, electron density (ED), electron energy density (EED), and electron current density (ECD).

2. Results and discussion

COMSOL Multiphysics plasma simulation program was used for modeling and evaluation of gas discharge–semiconductor systems (GDSS) in this research study.

A two-dimensional GDSS cell was conceptually designed and modeled with key elements including, cathode/anode electrode pair, microdischarge gap medium, and boundary walls. Direct-gap MCT semiconductor material was introduced as a planar cathode electrode in the cell. An optically transparent and electrically conductive tin dioxide (SnO_2) thin film was modeled on fused glass anode substrate.

A set of variables such as type and pressure of plasma process gas in the discharge medium, DC electrical equivalent circuit (DC-EEC) to drive GDSS cell, MCT cathode material with intrinsic parameters of work function, band gap, electron mobility has been introduced in the 2D-model. The related plasma reactions, cell boundary conditions, initial values, DC-EEC parameters have been introduced. In the study section of simulation platform, time-dependent computations were carried out in a well-defined output time range.

2D color surface images of spatiotemporal plasma patterns across micro-gap and line graphs of various discharge parameters including, electron density (ED), electron energy density (EED), and electron current density (ECD) were presented in 2D media. Fig. 4 shows the schematic of half-size GDSS cell with its dimensions in mm-scale ($r=x$, $\theta=0$, z).

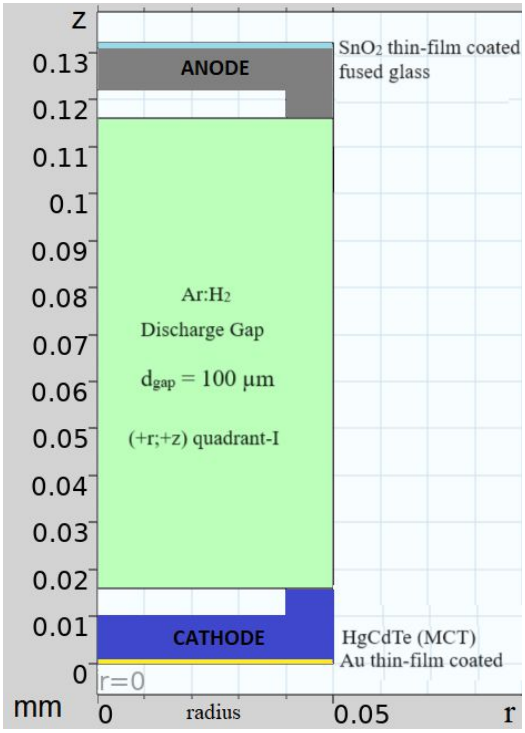

Fig. 4. Physical diagram of half-size GDSS cell with its dimensions in mm-scale (color online)

Fig. 5 shows the equivalent electrical circuit diagram of GDSS cell used in the simulation model.

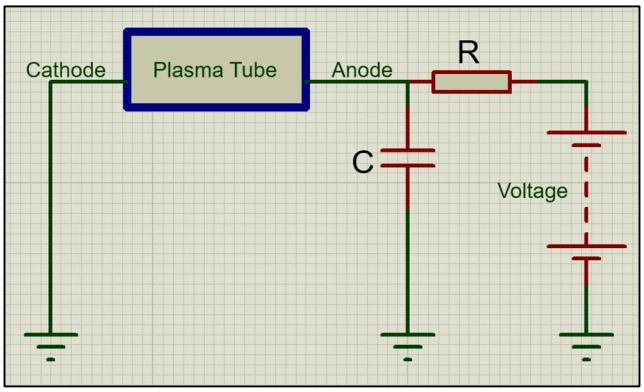

Fig. 5. Equivalent electrical circuit diagram of GDSS cell (color online)

The collision and ionization reactions in Table 1 were introduced in the simulation model.

Table 1. Collisions and ionization reactions of argon

Reaction	Formulas	Type	Δε (Ev)	
1	$e + Ar \longrightarrow e + Ar$	Elastic	0	Boltzmann
2	$e + Ar \longrightarrow 2e + Ar+$	Direct ionization	15.824	Boltzmann
3	$e + Ar \leftrightarrow e + Ar*$	Excitation	11.424	Boltzmann
4	$e + Ar \leftrightarrow e + Ar$	Excitation	13.1	Boltzmann
5	$e + Ar* \longrightarrow 2e + Ar+$	Stepwise ionization	4.3997	Boltzmann
6	$2Ar* \longrightarrow e + Ar+ + Ar$	Penning ionization	-	6.2×10^{-10} cm^3 s^{-1}
7	$Ar* \longrightarrow hv + Ar$	Radiation	-	$1.0\times10^{7}s^{-1}$

The spatiotemporal discharge parameters examined by this study are defined below for the proposed GDSS cell models with the conceptual design and simulation parameters:

Spatio-temporal discharge parameters:

- ❖ Electron Density (ED)
- ❖ Electron Energy Density (EED)
- ❖ Electron Current Density, *r*-component (ECD*r*)

Design and simulation parameters:

- Voltage source to drive GDSS cell models: V = 2.0 kV DC
- Gas discharge medium: Ar/H_2 mixture: Hydrogen is added to argon at 10% molar fraction.
- Process gas pressures: P_1 = 760 Torr (1 atm) and P_2 = 1,520 Torr (2 atm)
- Cathode electrode material: HgCdTe (MCT)
- Cathode electrode radius, r_{cath} = 50 µm
- Anode electrode material: Tin-dioxide (SnO_2) thin film on fused glass substrate
- Anode electrode radius, r_{anode} = 50 µm
- Interelectrode discharge gap length, d = 100 µm
- Operating ambient temperature of GDSS cell: T = 300 K
- 2D simulation study based on: The mixture-averaged diffusion-drift theory of gas discharges using the Maxwellian electron energy distribution function in COMSOL Multiphysics DC Plasma Program.

I. Electron Density (ED)

Fig. 6 shows "Electron Density (ED)" simulation results of GDSS cell models in Ar/H_2 media at pressures of (a-c) 760 Torr and (b-d) 1,520 Torr, respectively. 2D surface images of spatiotemporal ED parameter (c-d) were rendered in rainbow-classic color range across micro-gap at the indicated output times of plasma process.

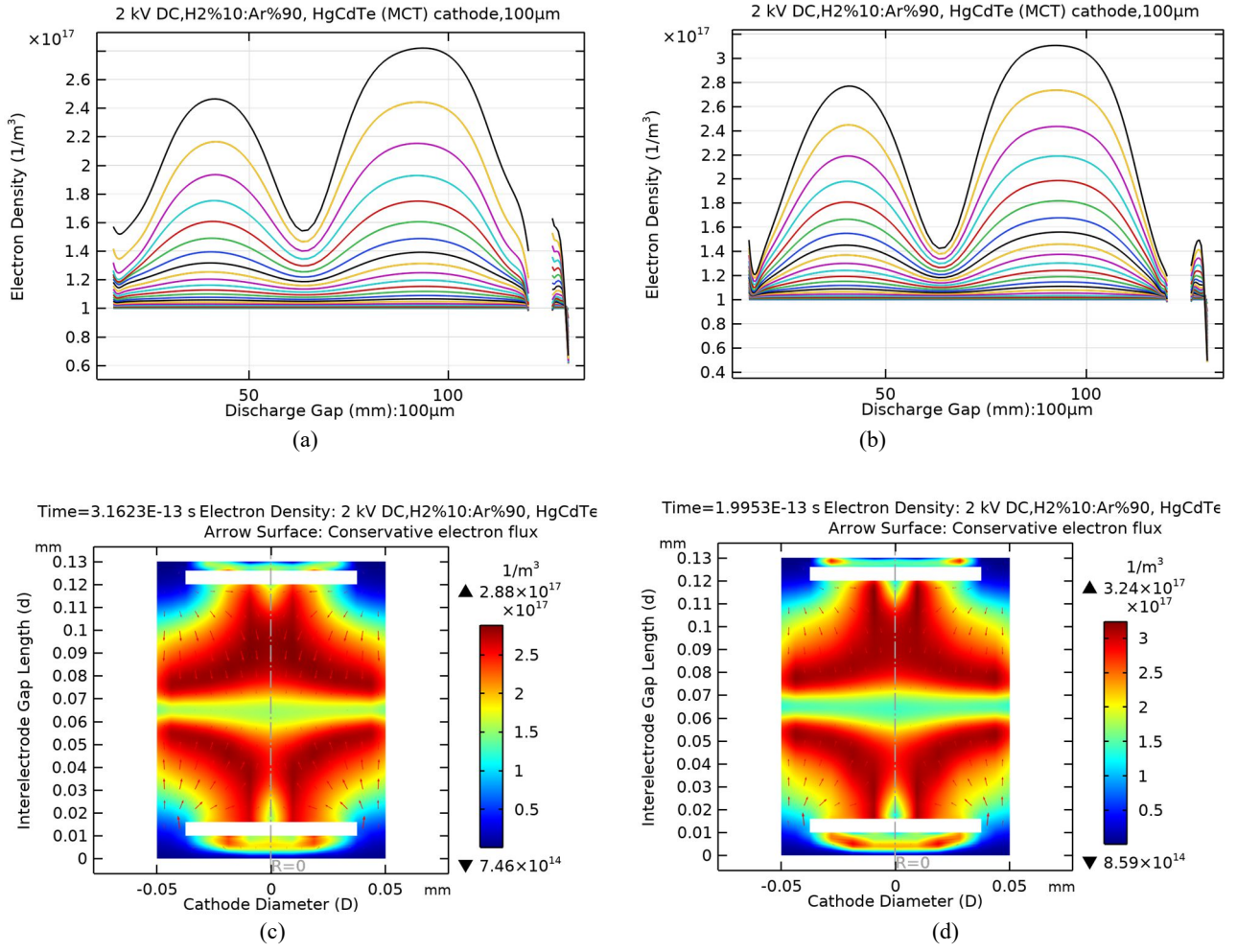

Fig. 6. Electron Density (ED) simulation results of GDSS cell models in Ar/H_2 media: (a) 1D-ED curves formed throughout the plasma process at 760 Torr, (b) 1D-ED curves formed throughout the plasma process at 1,520 Torr, (c) 2D-ED plasma surface pattern formed at output time of 3.1623E-13s at 760 Torr, (d) 2D-ED plasma surface pattern formed at output time of 1.9953E-13s at 1,520 Torr (color online)

II. Electron Energy Density (EED)

Fig. 7 shows "Electron Energy Density (EED)" simulation results of GDSS cell models in Ar/H_2 media at pressures of (a-c) 760 Torr and (b-d) 1,520 Torr, respectively. 2D surface images of spatiotemporal EED parameter (c-d) were rendered in rainbow-classic color range across micro-gap at the indicated output times of plasma process.

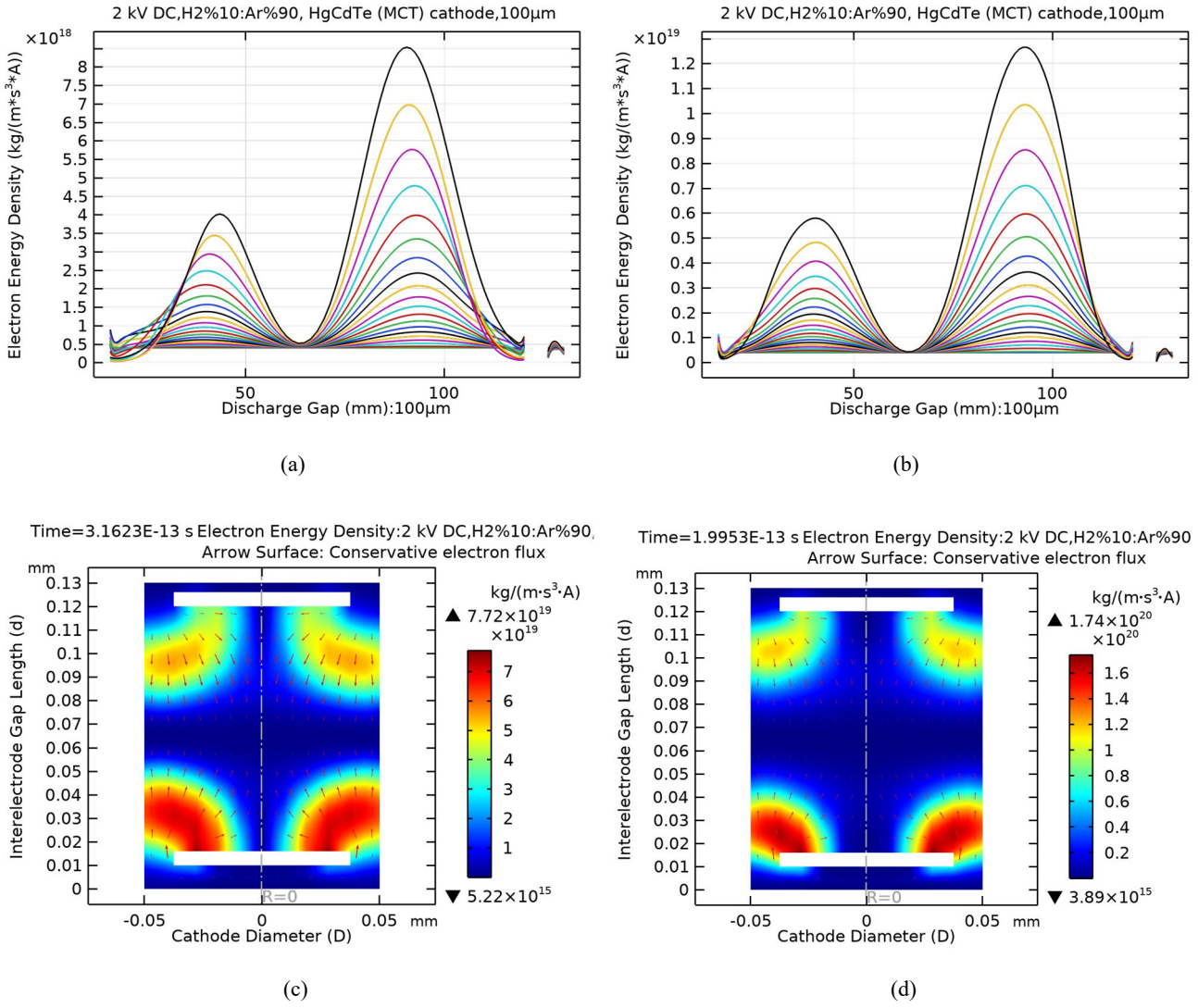

Fig. 7. Electron Energy Density (EED) simulation results of GDSS cell models in Ar/H_2 media: (a) 1D- EED curves formed throughout the plasma process at 760 Torr, (b) 1D- EED curves formed throughout the plasma process at 1,520 Torr, (c) 2D- EED plasma surface pattern formed at output time of 3.1623E-13s at 760 Torr, (d) 2D- EED plasma surface pattern formed at output time of 1.9953E-13s at 1,520 Torr (color online)

III. Electron Current Density, *r*-component (ECD*r*)

Fig. 8 shows "Electron Current Density, *r*-component (ECD*r*)" simulation results of GDSS cell models in Ar/H_2 media at pressures of (a-c) 760 Torr and (b-d) 1,520 Torr, respectively. 2D surface images of spatiotemporal ECD*r* parameter (c-d) were rendered in rainbow-classic color range across micro-gap at the indicated output times of plasma process.

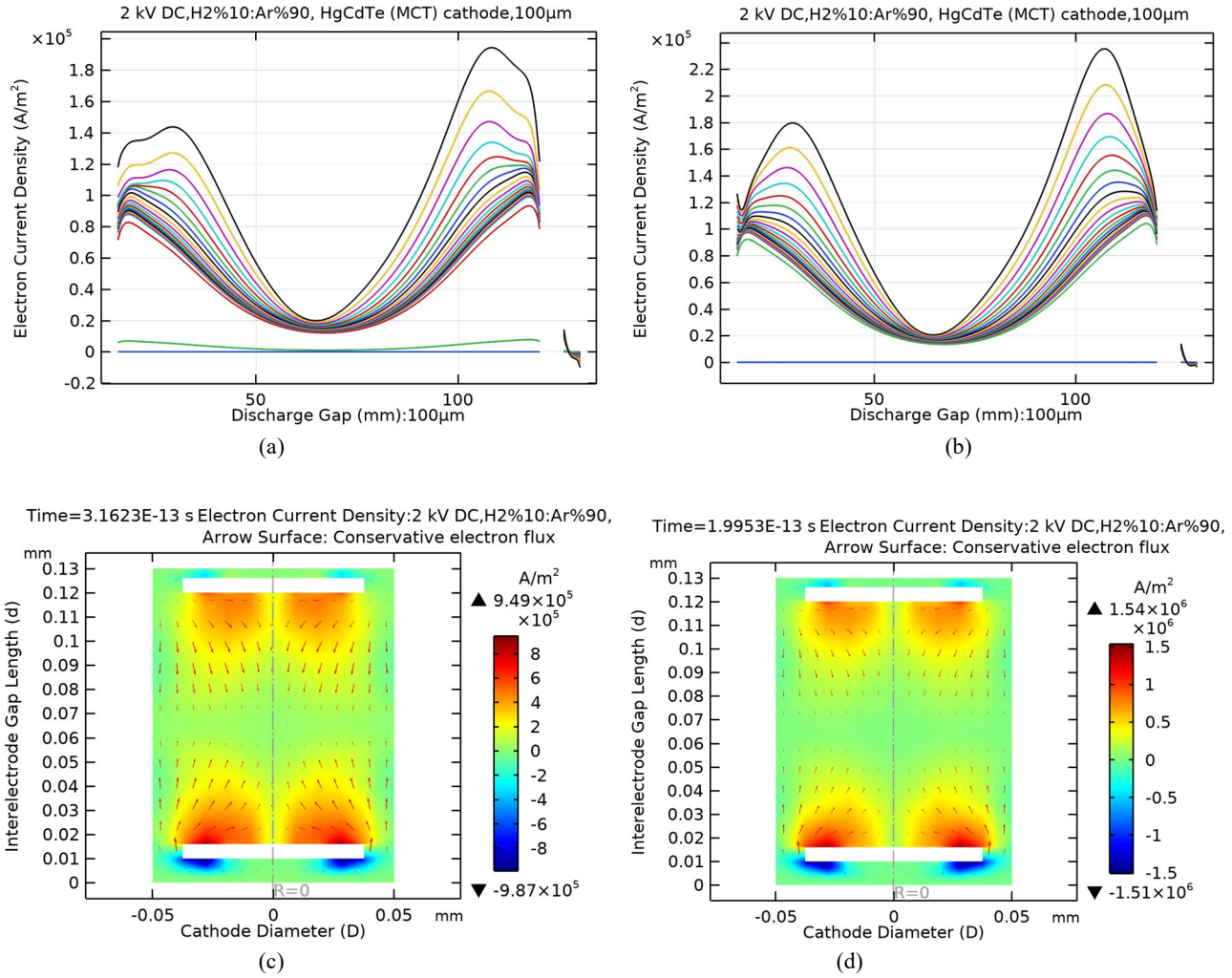

Fig. 8. Electron Current Density, r-component (ECDr) simulation results of GDSS cell models in Ar/H2 media: (a) 1D- ECDr curves formed throughout the plasma process at 760 Torr, (b) 1D- ECDr curves formed throughout the plasma process at 1,520 Torr, (c) 2D-ECDr plasma surface pattern formed at output time of 3.1623E-13s at 760 Torr, (d) 2D- ECDr plasma surface pattern formed at output time of 1.9953E-13s at 1,520 Torr (color online)

For each cell model of GDSS, the spontaneous values of three major discharge parameters (ED, EED, ECD) calculated at specified output times of plasma transition period are given in Table 2.

Table 2. Discharge parameters obtained from 2D-simulation results

GDSS model	Ar/H_2 pressure	Output Time	Electron Density ED ($1/m^3$)	Electron Energy Density EED peak ($kg/(m.s^3.A)$)	Electron Current Density, radial ECD*r* (A/m^2)
2.0 kV DC -driven HgCdTe (MCT) Ar/H_2(10%)	760 Torr	3.1623E-13 s	2.88E17	8.5E18	1.95E5
	1,520 Torr	1.9953E-13 s	3.24E17	1.27E19	2.35E5

Following, for each cell model of GDSS, the Peak Electron Current Ratings (*p*ECRs) in the cell at 760 Torr and 1,520 Torr were manually calculated by using the spontaneous Electron Current Density (ECD*r*) data in Table 3. The peak ECR data are located on the characteristic I-V curve to approximately indicate the operating point of each GDSS model in Fig. 9.

Table 3. The calculated electron currents at two-different pressures upon GDSS simulations

Pressure of binary Ar/H_2 gas medium	760 Torr	1,520 Torr
Specified Output Time (s) in the plasma transition period	3.1623E-13	1.9953E-13
Electron Current Density, ECD*r* (kA/m^2)	195	235
2D-microplasma discharge cell area (μm^2)	100 μm × 100 μm	
Peak Electron Current Rating, *p*ECR (mA)	1.95	2.35

In Fig. 9, the characteristic current/voltage (I/V) curve of a typical gas discharge system including, dark discharge, glow discharge and arc discharge regimes is introduced [30, 31].

The Peak Electron Current Rating (*p*ECR) of binary Ar/H_2 gas system at 1,520 Torr hyper-atmospheric pressure increased to approximately 2.35 mA from 1.95 mA at 760 Torr atmospheric pressure.

In this numerical study, the I/V operating points of both GDSS cell models were calculated to be around 2.0 mA; which is shown through the solid vertical projection line in blue in the normal glow discharge regime as shown in Fig. 9.

Fig. 10 shows the Paschen curves for argon and hydrogen gases [31]. Pressures of Ar/H_2 gas mixture was set at P_1=760 Torr and at P_2=1,520 Torr, discharge gap length was fixed at d = 100 μm, and the products of $P_1 \cdot d$ = 7.6 Torr·cm and $P_2 \cdot d$ = 15.2 Torr·cm were located on the Paschen curves to roughly estimate the DC breakdown voltage change depending on the gas mixture type and pressure [32-34].

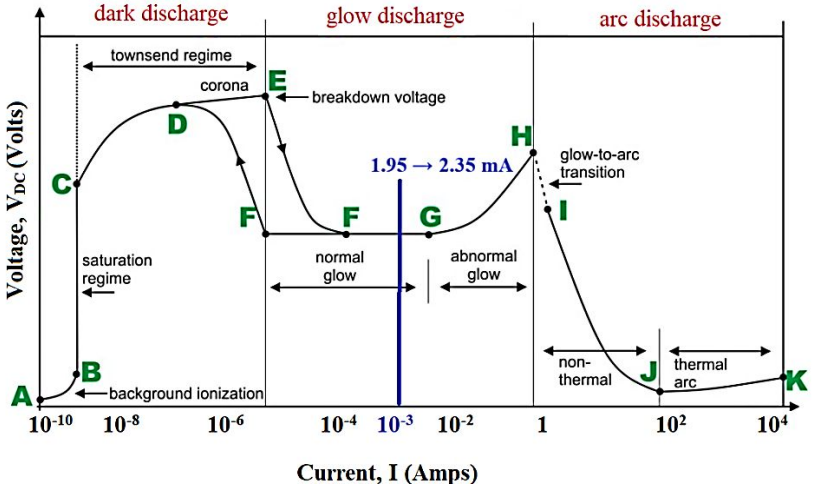

Fig. 9. Current/Voltage (I/V) curve of a typical gas discharge system [30, 31]. The calculated operating points of the simulated cell models are located around the solid vertical projection line in blue at approximately 2.0 mA (online color)

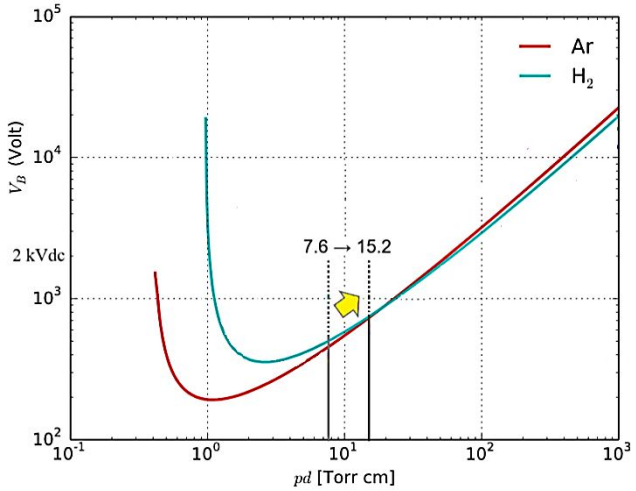

Fig. 10. Paschen curves for Ar and H_2 gases [31]. Pressures of Ar/H_2 gas mixture were set at P_1=760 Torr and at P_2=1,520 Torr, discharge gap length was set at d = 100 μm, and the products of $P_1 \cdot d$ = 7.6 Torr·cm and $P_2 \cdot d$ = 15.2 Torr·cm located on the Paschen curves to estimate DC breakdown voltage change depending on the gas mixture pressure (color online)

The self-breakdown voltage (SBV) of binary Ar/H_2 gas system at hyper-atmospheric pressure has elevated to approximately 1.0 kV DC from around 0.5 kV DC at atmospheric pressure.

3. Conclusions

This research study aimed to identify the unique transition regimes between electron emission and gas breakdown mechanism across a micro gap, and to truly model the basis of high-efficiency infrared-visible wavelength conversion devices.

The optical and electrical characteristics of direct current glow discharges strictly depend on numerous key parameters including, cathode material, process gas medium and pressure, interelectrode gap length, electrical equivalent circuit, self-breakdown voltage (SBV), and dimensions of plasma reactor chamber.

The Gas Discharge-Semiconductor System (GDSS) cell models with direct bandgap HgCdTe (MCT) semiconductor material -coupled to Ar/H_2 gas media were studied at 760 Torr atmospheric and 1,520 Torr hyper-atmospheric pressures using the COMSOL Multiphysics simulation platform and the Finite Element Method (FEM) numerical modeling technique for finding approximate solutions to boundary value problems for differential equations. Numerical analysis results of the spatiotemporal discharge parameters including, electron density (ED), electron energy density (EED), and electron current density (ECD) obtained from the Gas Discharge Semiconductor System (GDSS) simulation models have revealed that a significant contribution can be made to increasing ion-induced secondary electron emission (SEE) yield in hydrogen-added argon gas medium at hyper-atmospheric pressure.

The Peak Electron Current Rating (*p*ECR) of binary Ar/H_2 gas system at 1,520 Torr hyper-atmospheric pressure increased to approximately 2.35 mA from 1.95 mA at 760 Torr atmospheric pressure. The calculated operating points of both GDSS models are located at around 2.0 mA in the normal glow discharge regime. The self-breakdown voltage (SBV) of binary Ar/H_2 gas system at hyper-atmospheric pressure elevated to approximately 1.0 kV DC from around 0.5 kV DC at atmospheric pressure.

The simulation studies with numerical analysis results of this research established a strong theoretical basis to design the experimental models. Next, it is planned to focus on the experimental investigations including, spectral response, sensitivity to NIR/MWIR spectra, and energy conversion efficiency of the proposed GDSS cell model.

Acknowledgement

This study was supported by Gazi University, Scientific Research Project Coordination Unit with grand numbers FDK-2023-8704 and FDK-2023-8701.

Declaration of ethical standards

The authors declare that the materials and methods used in this study do not require ethical committee permission and/or legal-special permission.

Authors' contributions

Prof. Dr. Hatice Hilal YÜCEL (KURT): Expert in theoretical and experimental plasma physics, modeling, simulation, article writing and editing.

Erhan ONGUN: Modeling, simulation, article writing.

Selçuk UTAŞ: Modeling, simulation.

Conflict of interest statement

The authors declare no conflict of interest in this study.

Data availability statement

The data that support the findings of this study are available on request from the corresponding author.

References

[1] H. H. Kurt, B. G. Salamov, JOM **72**, 651 (2020).
[2] W.-H. Chiang, D. Mariotti, R. M. Sankaran, J. G. Eden, K. Ostrikov, Adv. Mater. **32**, 1905508 (2020).
[3] M. Kong, G. Kroesen, G. Morfill, T. Nosenko, T. Shimizu, J. Van Dijk, J. L. M. Zimmermann, New J. Phys. **11**, 115012 (2009).
[4] K. H. Schoenbach, K. Becker, Eur. Phys. J. D. **70**, 29 (2016).
[5] T. von Woedtke, M. Laroussi, M. Gherardi, Plasma Sources Science and Technology **31**, 054002 (2022).
[6] M. M. Bülbül, H. H. Kurt, B. G. Salamov, 7th Int'l Conference on Nanometer-Scale Science and Technology (ECOSS-21), Malmö, Sweden (2002).
[7] H. Y. Kurt, A.İnalöz, B. G. Salamov, Optoelectron. Adv. Mat. **4**(2), 205 (2010).
[8] A. L. Garner, A. M. Loveless, J. N. Dahal, A. Venkattraman, IEEE Trans. Plasma Sci. **48**, 808 (2020).
[9] O. P. Agnihotri, H. C. Lee, K. Yang, Semiconductor Science and Technology **17**(10), R11 (2002).
[10] M. Carmody, D. Edwall, J. Ellsworth, J. Arias, M. Groenert, R. Jacobs, L. A. Almeida, J. H. Dinan, Y. Chen, G. Brill, N. K. Dharr, J. Electron. Mater. **36**, 1098 (2007).
[11] P. M. Amirtharaj, J. H. Burnett, Narrow-gap II-VI Compounds for Optoelectronic and Electromagnetic Applications, Chapman and Hall, London, 1 edition (1997).
[12] S. D. Guapala, S. V. Bandara, Semiconductors and Semimetals **62**, 197 (1999).
[13] M. Razeghi, A. Dehzangi, J. Li, Results in

Optics **2**(1), 100054 (2021).
[14] M. A. Kinch, Journal of Electronic Materials **29**, 809 (2000).
[15] P. Norton, Opto-Electronics Review **10**(3), 159 (2002).
[16] F. Gemain, I. C. Robin, S. Brochen, M. De Vita, O. Gravrand, A. Lusson, Journal of Electronic Materials **41**, 2867 (2012).
[17] J. Polit, Bulletin of the Polish Academy of Sciences Technical Sciences **59**(3), 331 (2011).
[18] R. W. Birkmire, B. E. McCandless, Curr. Opin. Solid State Mater. Sci. **14**(6), 139 (2010).
[19] M. Günnar, Characterization of molecular beam epitaxially crown CdTe layers over GaAs by spectroscopic ellipsometry (Doctoral dissertation, Izmir Institute of Technology) (2014).
[20] M. A. Kinch, J. D. Beck, C. F. Wan, F. Ma, J. Campbell, Journal of Electronic Materials **33**(6), 630 (2004).
[21] M. Kopytko, W. Gawron, A. Kębłowski, D. Stępień, P. Martyniuk, K. Jóźwikowski, Optical and Quantum Electronics **51**, article nr. 62 (2019).
[22] J. Chen, J. Wang, X. Li, J. Chen, F. Yu, J. He, J. Wang, Z. Zhao, G. Li, X. Chen, W. Lu, Sensors **22**(2), 677 (2022).
[23] A. L. Garner, G. Meng, Y. Fu, J. Appl. Phys. **128**, 210903 (2020).
[24] H. H. Kurt, E. Tanrıverdi, Journal of Electronic Materials **46**, 4024 (2017).
[25] Y. Fu, P. Zhang, J. P. Verboncoeur, X. Wang, Plasma Res. Express **2**(1), 013001 (2020).
[26] D. B. Go, A. Venkattraman, J. Phys. D Appl. Phys. **47**, 503001 (2014).
[27] J. W. Coburn, W. W. Harrison, Trans. R. Soc. **171**, 65 (1981).
[28] J-L. Delcroix, A. R. Trindade, Advances in Electronics and Electron Physics **35**, 87 (1974).
[29] H. H. Kurt, E. Tanrıverdi, Journal of Electronic Materials **46**, 3965 (2017).
[30] J. L. Vossen, Thin Film Processes, Academic Press Inc., New York (1978).
[31] T. A. Massood, P. Pradeep, Micromachines **8**(4), 117 (2017).
[32] M. Klas, Š. Matejčik, B. Radjenović, M. Radmilović-Radjenović, Physics Letters A **376**(10-11), 1048 (2012).
[33] E. Ongun, H.H. Yücel (Kurt), S. Utaş, J. Mater. Sci.: Mater. Electron. **35**, 655 (2024).
[34] Y. Sadiq, H. Yücel Kurt, B.G. Salamov, J. Phys. D: Appl. Phys. **41**, 225204 (2008).

*Corresponding author: hkurt@gazi.edu.tr